Supporting Information

Electronic-Structure Regulation of Graphdiyne-Supported Dual-Atom Catalysts Drives Efficient Urea Synthesis from CO_2 and N_2

Rongxin Zhang[1#], Qingshuang Ma[1#], Haiyi Zhang[1#], Weiyi Wang[1], Lijuan Yu[1], Qineng Xia[1], Haiyan Wang[2], Suiqin Li[3*], Xiang Sun[4*], Yongyong Cao[1*]*

1 College of Biological, Chemical Science and Engineering, Jiaxing University, Jiaxing 314001, Zhejiang, P.R.China

2 Key Laboratory of the Ministry of Education for Advanced Catalysis Materials, Department of Chemistry, Zhejiang Normal University, Jinhua 321004, Zhejiang, P.R.China

3 Zhejiang Key Laboratory of Functional ionic membrane Materials and Technology for Hydrogen Production, Shaoxing University, Shaoxing 312000, Zhejiang, P.R.China

4 Zhejiang Research Institute of Chemical Industry Co.,Ltd, Hangzhou, 310052 Zhejiang, P.R.China

** Corresponding author：*
Email address: chemwhy@zjnu.edu.cn (H. Wang); lisq@usx.edu.cn (S. Li); sunxiang6@sinochem.com (X. Sun); cyy@zjxu.edu.cn (Y. Cao);

 # These authors contributed equally to this work;

Content

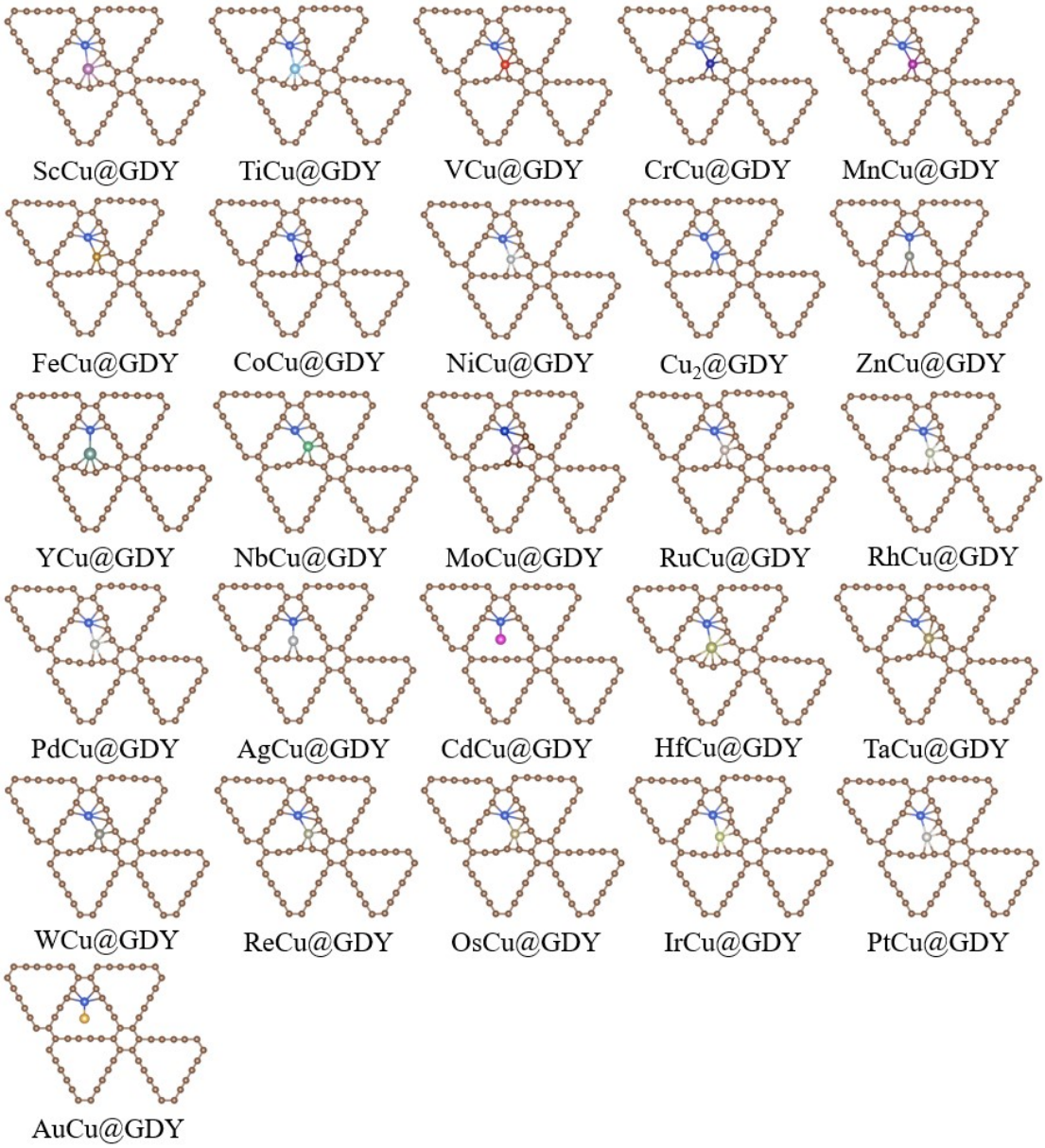

Figure S1. The optimized geometries of 26 transition-metals and Cu anchored graphdiyne (TMCu@GDY) configurations.

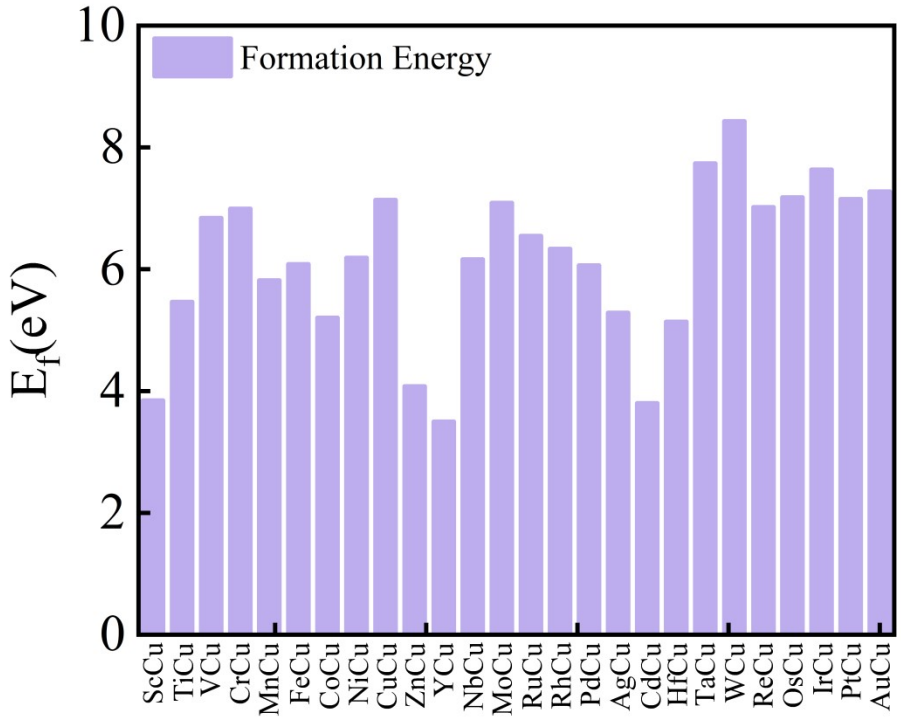

Figure S2. The formation energy (E_f) of 26 catalysts with bimetallic atom transfer charges.

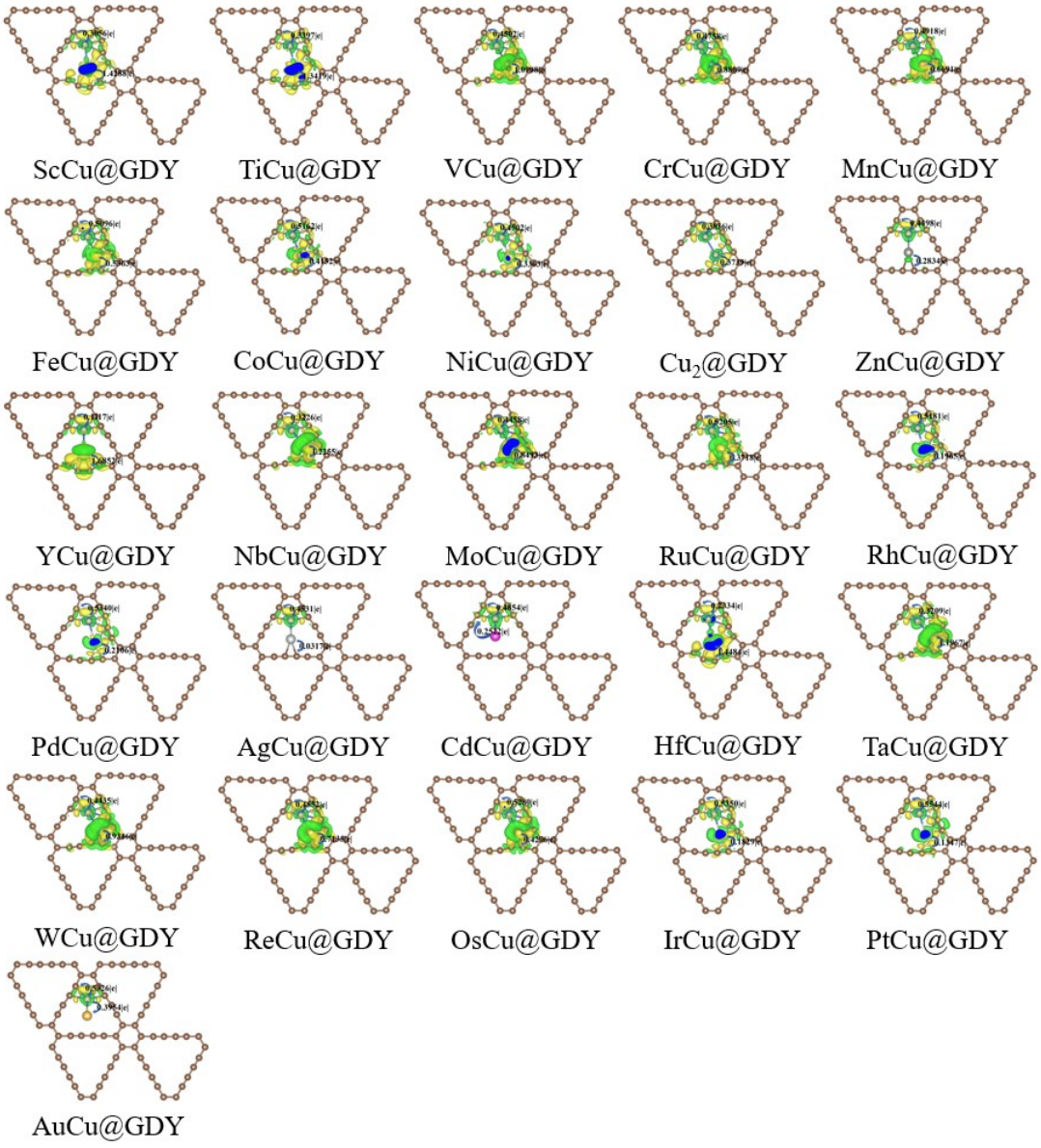

Figure S3. The charge density difference (CDD) for 26 stable TMCu@GDY with an isosurface value of 0.005 e/Å^{-3}, the charge accumulation and depletion were depicted by green and yellow, respectively.

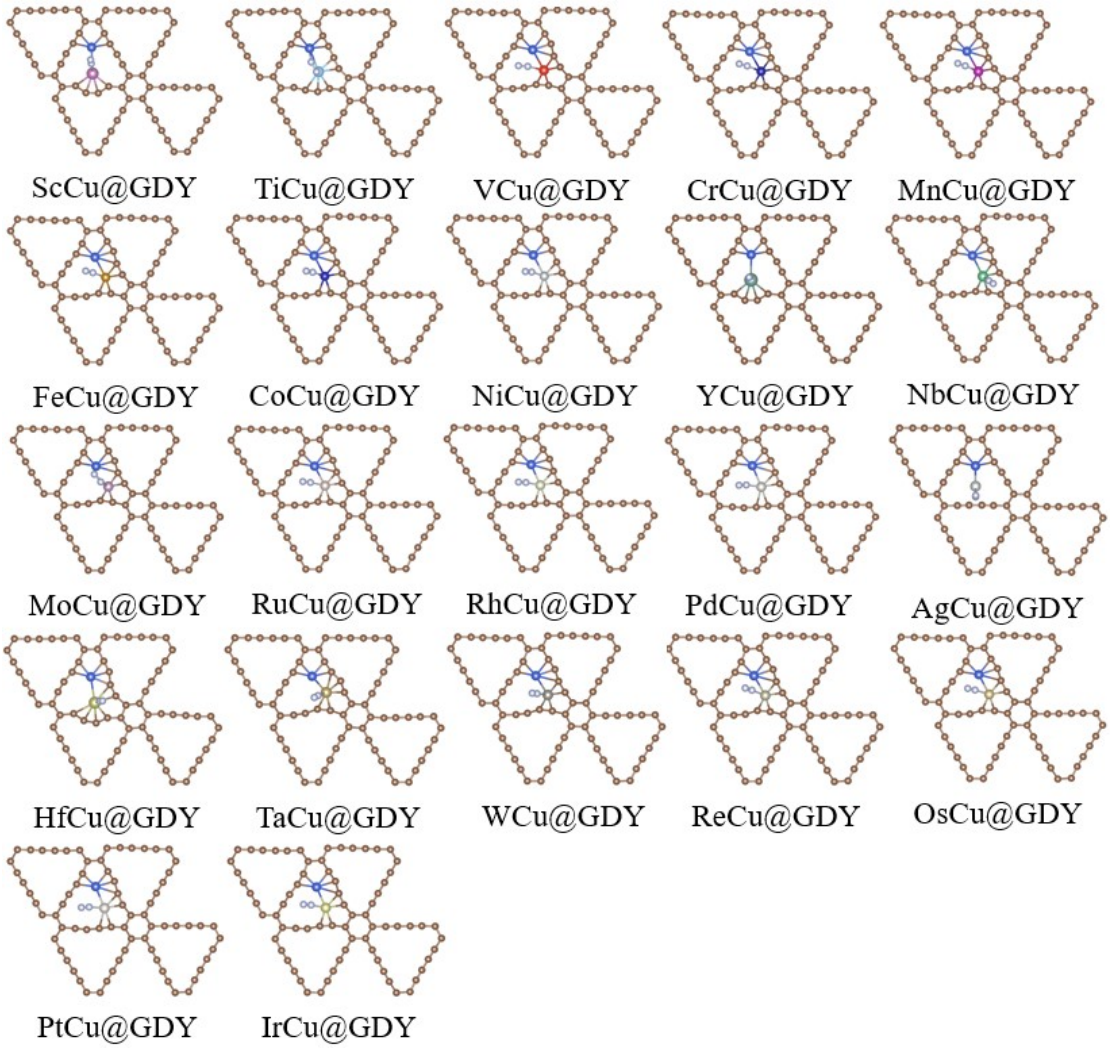

Figure S4. The optimized configurations of $*N_2$ spontaneously adsorbed on the TMCu@GDY.

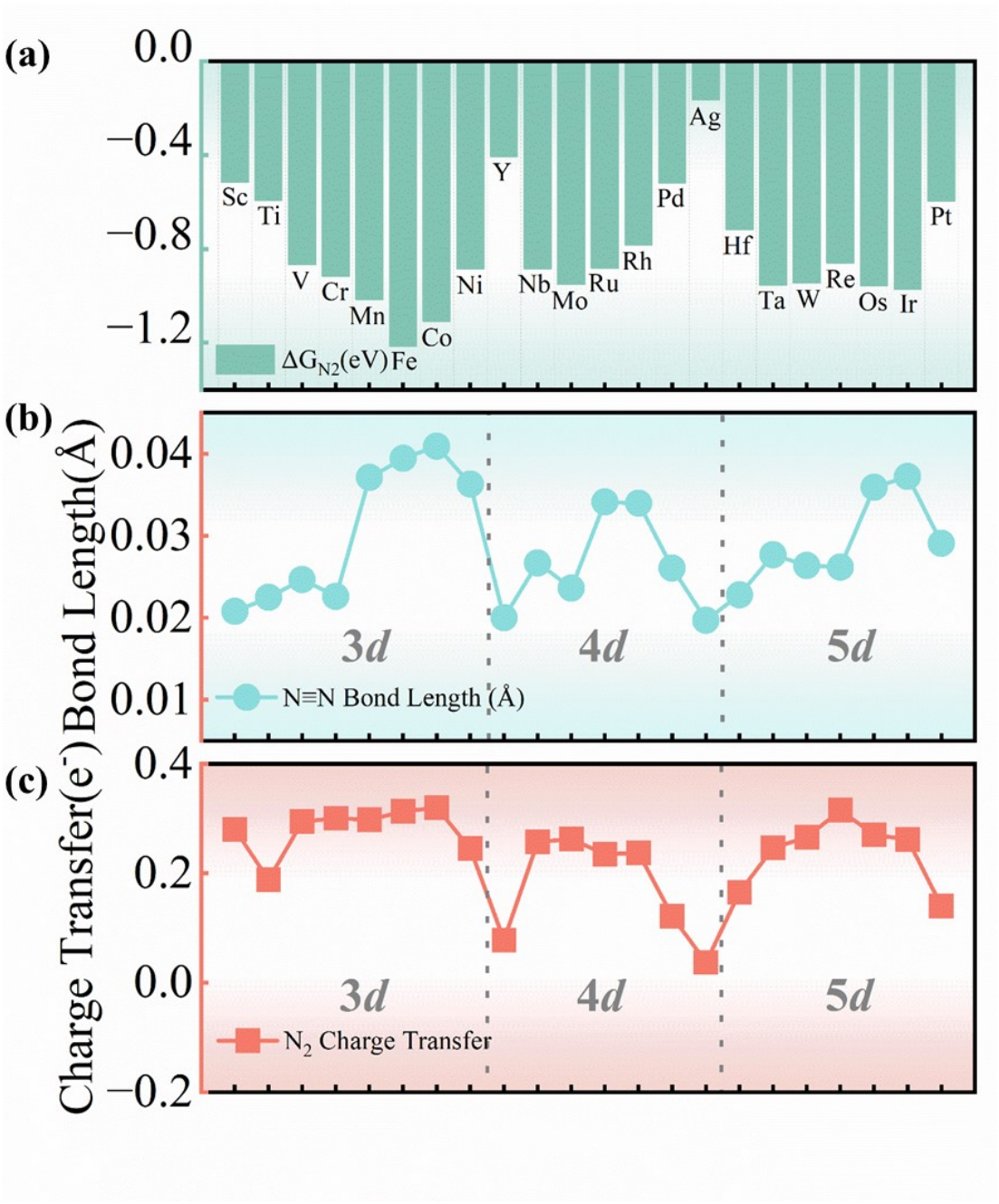

Figure S5. (a) Adsorption free energy, (b) the change of N≡N bond length, (c) electron gain/loss of adsorbed *N_2 on DACs.

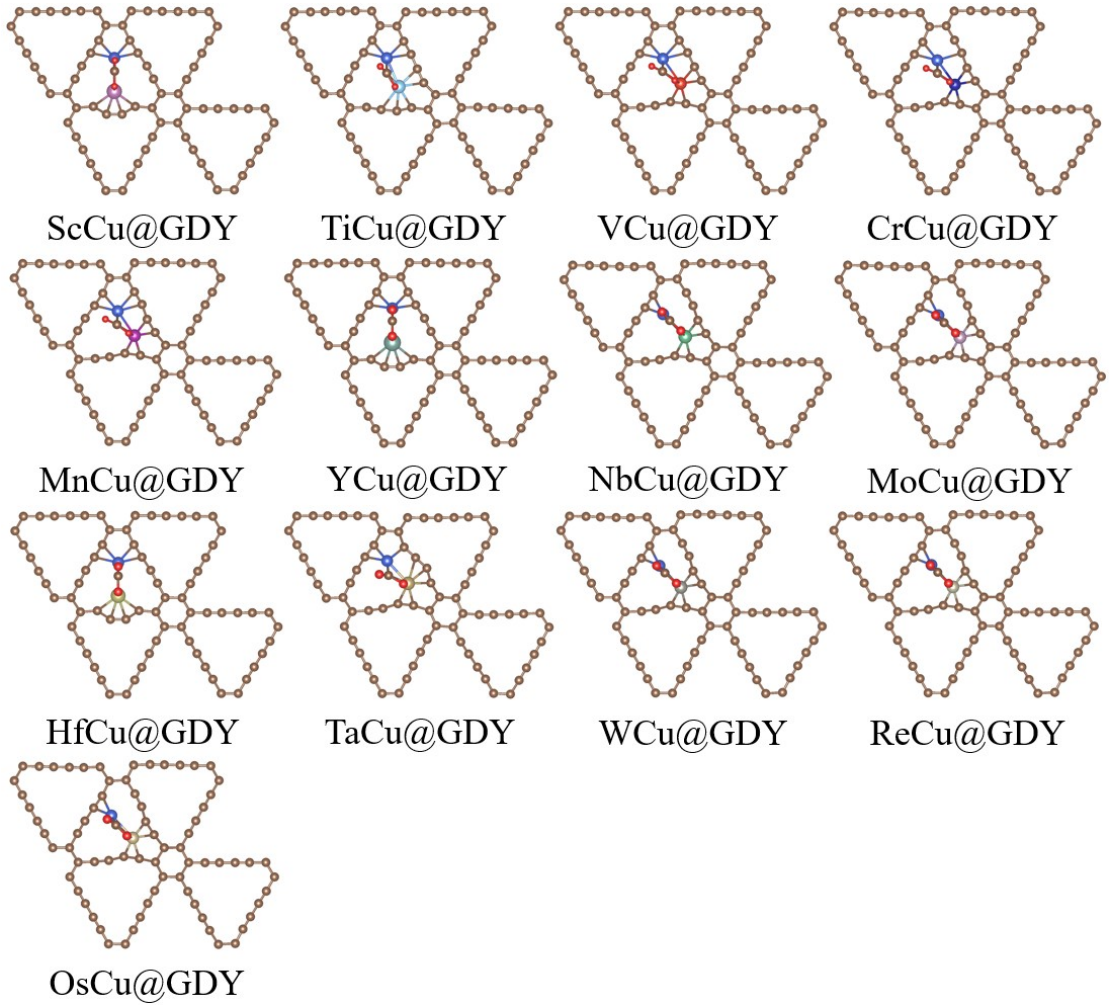

Figure S6. The optimized configurations of *CO_2 spontaneously adsorbed on the TMCu@GDY.

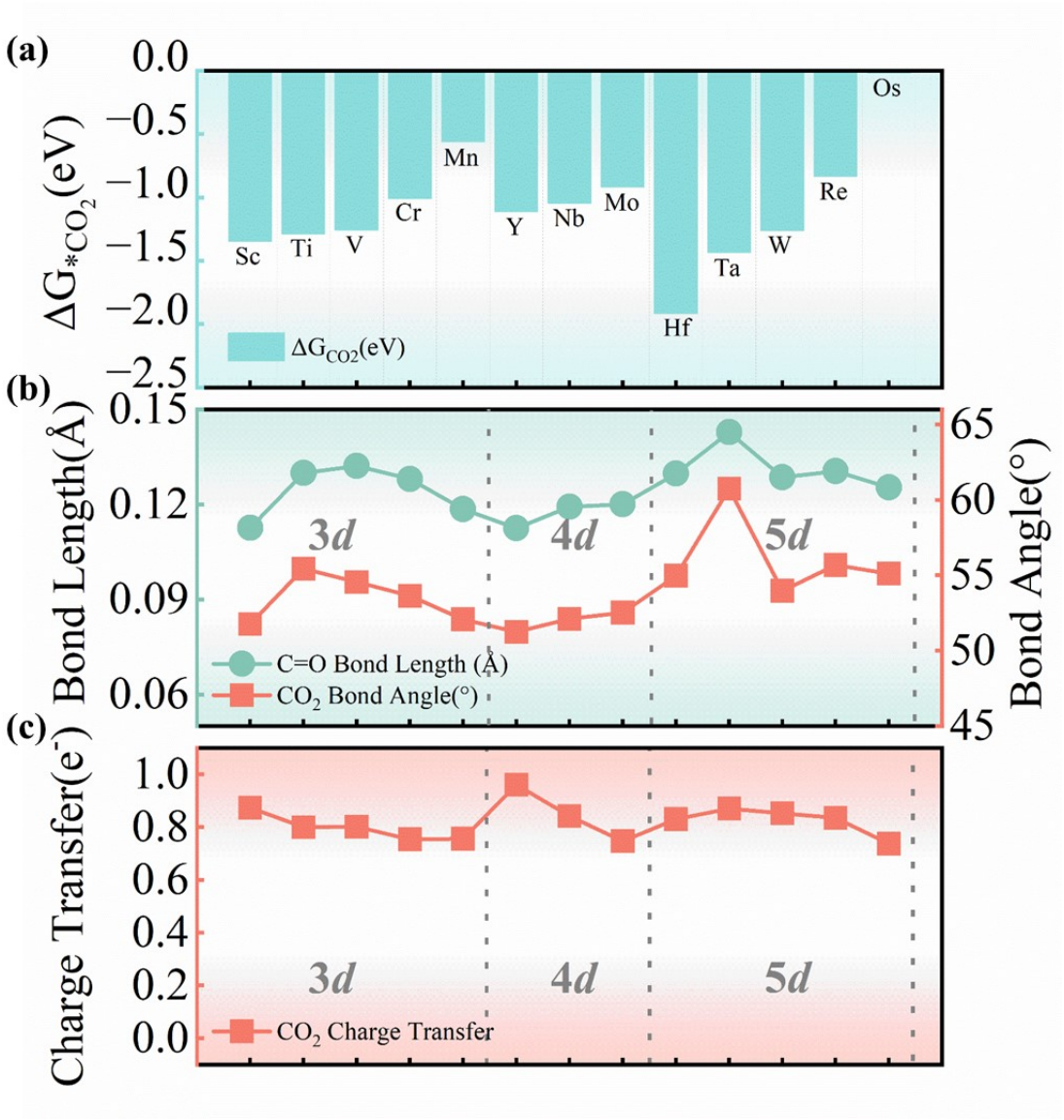

Figure S7. (a) Adsorption free energy, (b) the change of bond length, bond angle, (c) electron gain/loss of adsorbed *CO_2 on DACs.

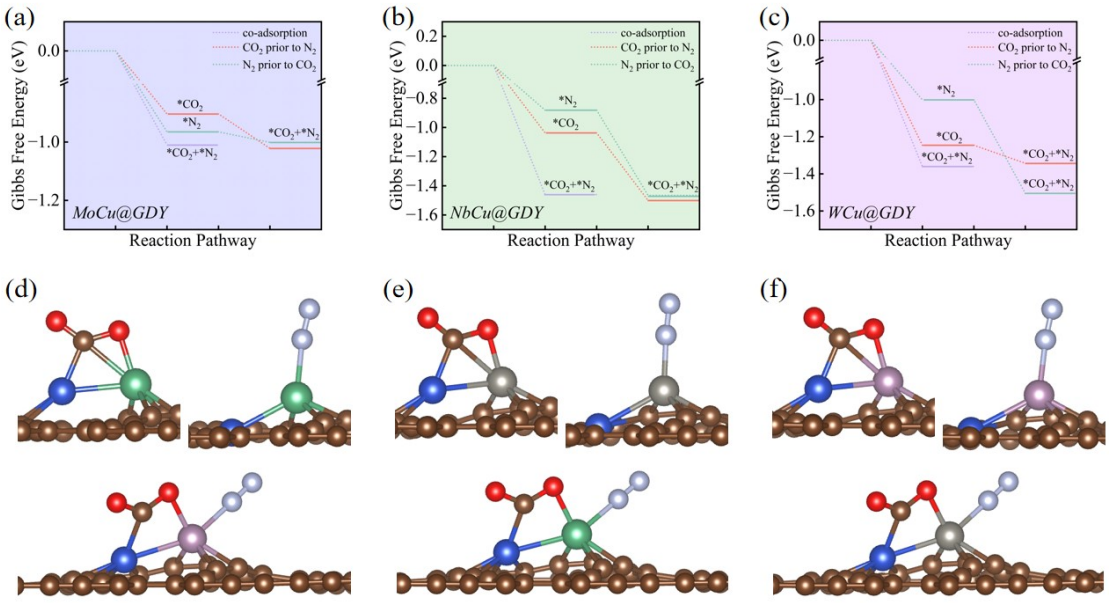

Figure S8. (a)-(c) represent the adsorption energies for Mo@GDY, Nb@GDY, and W@GDY, respectively, under two-step and one-step adsorption conditions. (d)-(f) depict the optimised intermediates corresponding to the adsorption processes.

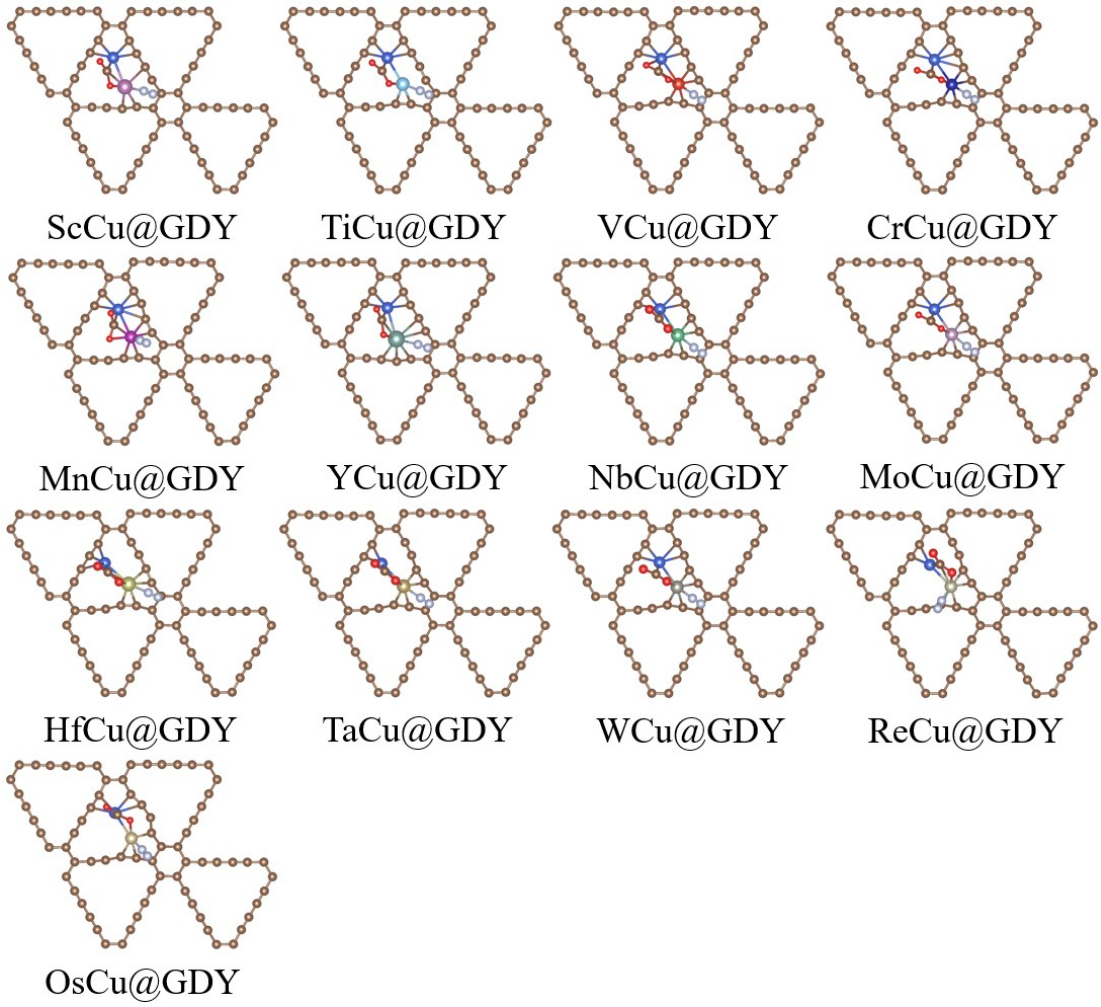

Figure S9. The optimized configurations of *CO_2 and *N_2 spontaneously adsorbed on the TMCu@GDY.

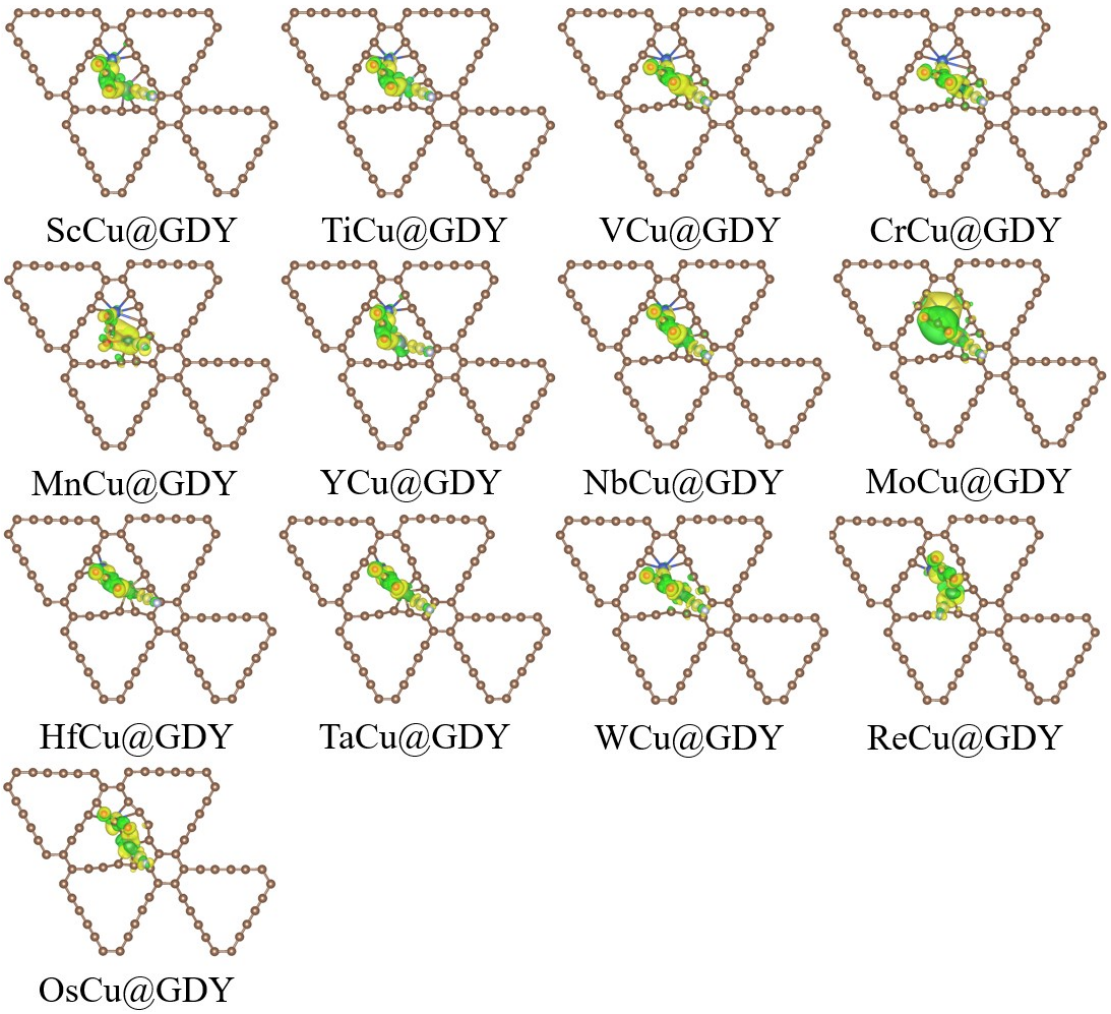

Figure S10. The CDD of $*CO_2$ and $*N_2$ adsorbed on the TMCu@GDY with an isosurface value of 0.005 e/Å^{-3}, the charge accumulation and depletion were depicted by green and yellow, respectively.

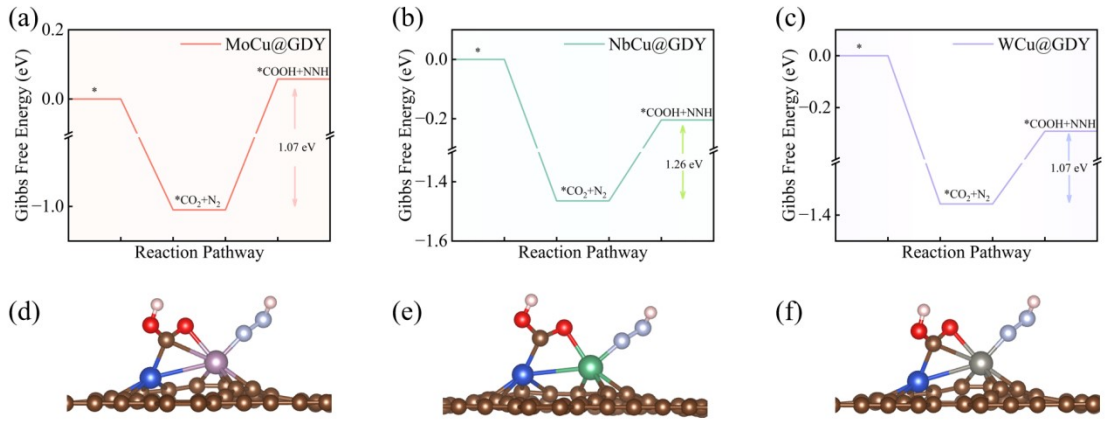

Figure S11. (a)-(c) Gibbs free-energy profiles for the simultaneous hydrogenation pathway of co-adsorbed CO_2 and N_2 on MoCu@GDY, NbCu@GDY, and WCu@GDY. (d)-(f) *COOH+NNH optimized intermediates on MoCu@GDY, NbCu@GDY, WCu@GDY.

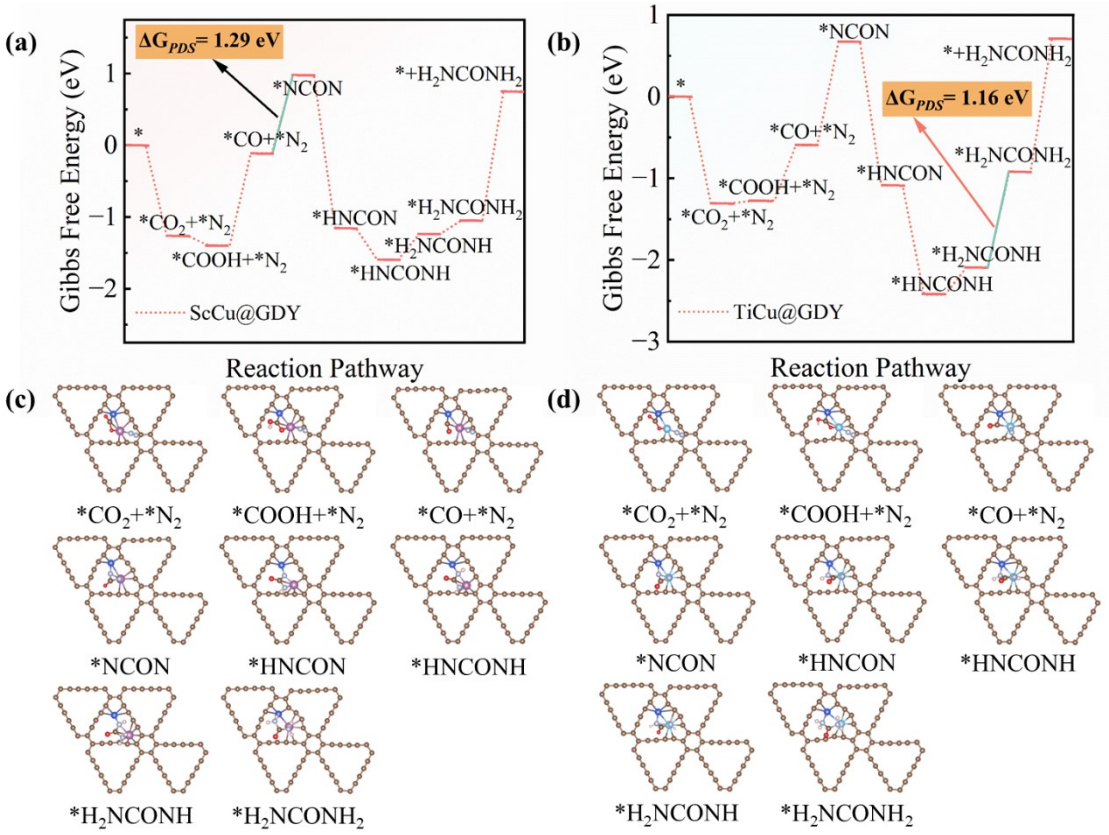

Figure S12. (a)-(b) Gibbs free energy diagrams of urea synthesis on ScCu@GDY and TiCu@GDY, (c)-(d) Optimized intermediate configurations for urea synthesis on ScCu@GDY and TiCu@GDY.

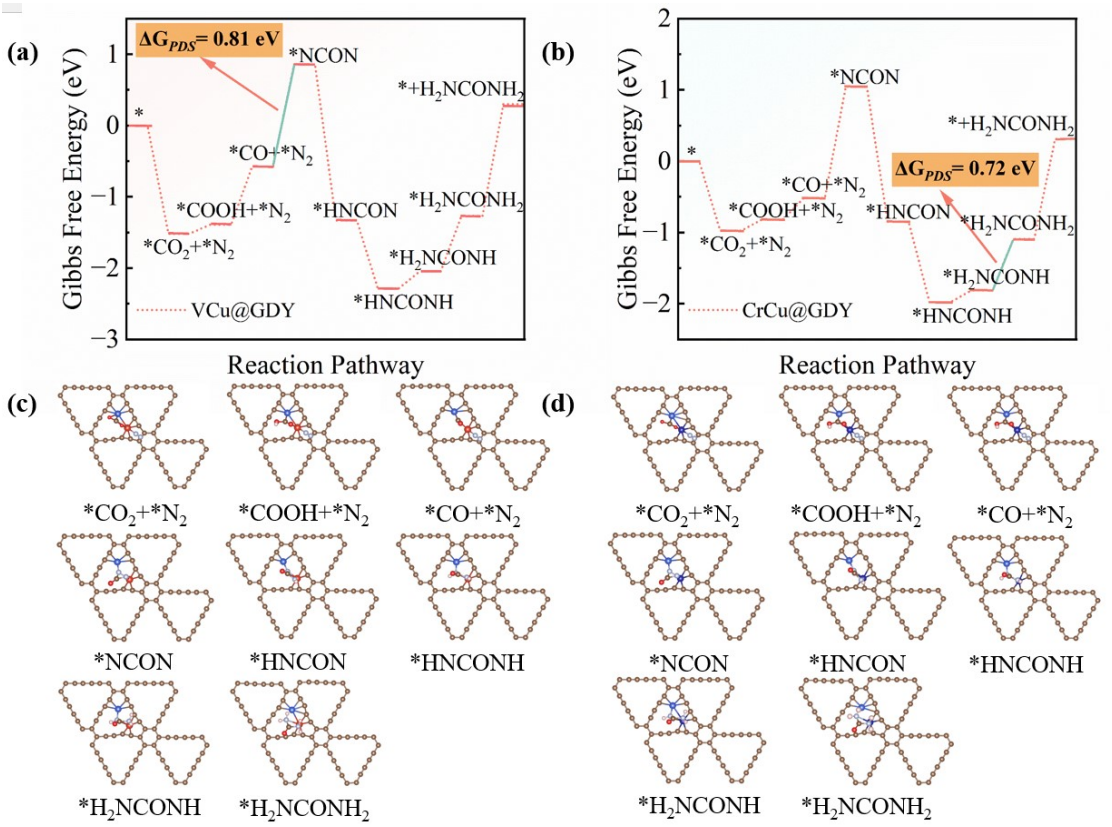

Figure S13. (a)-(b) Gibbs free energy diagrams of urea synthesis on VCu@GDY and CrCu@GDY, (c)-(d) Optimized intermediate configurations for urea synthesis on VCu@GDY and CrCu@GDY.

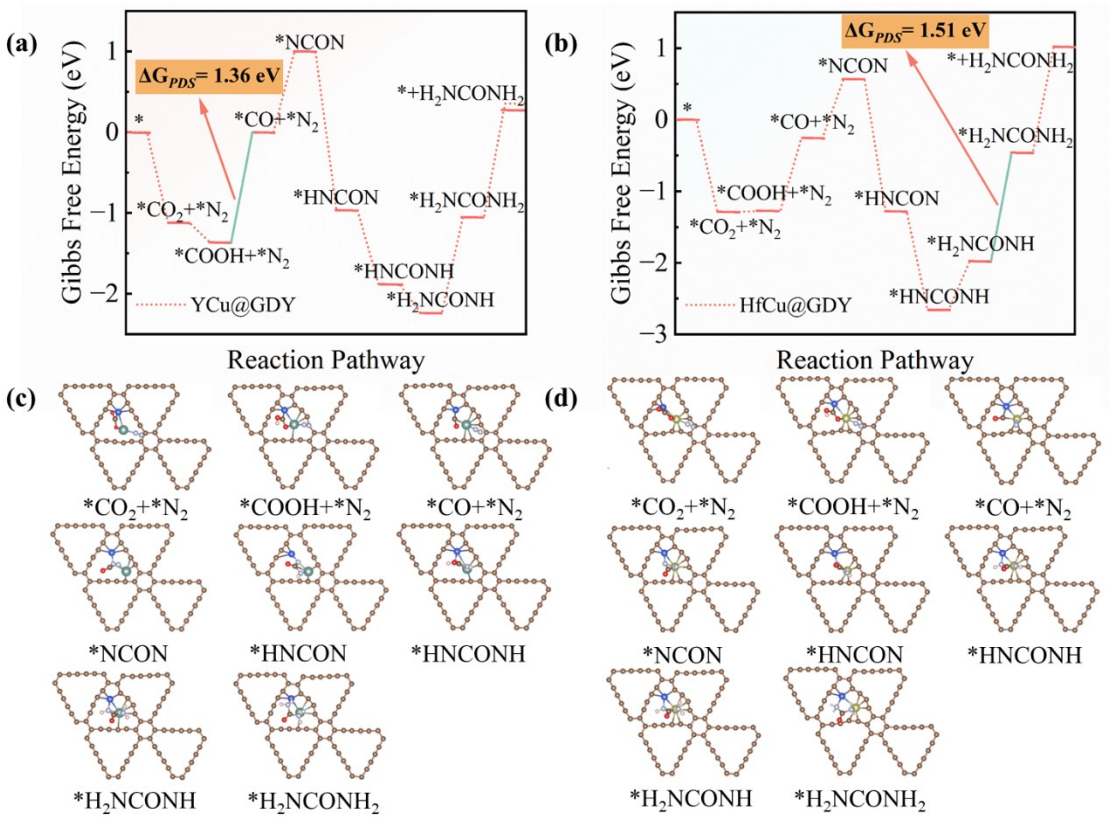

Figure S14. (a)-(b) Gibbs free energy diagrams of urea synthesis on YCu@GDY and HfCu@GDY, (c)-(d) Optimized intermediate configurations for urea synthesis on YCu@GDY and HfCu@GDY.

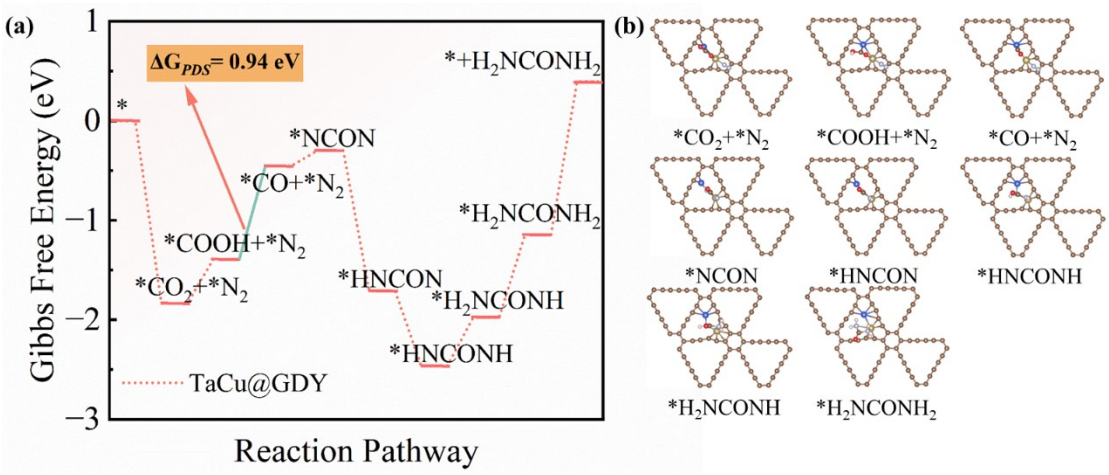

Figure S15. (a) Gibbs free energy diagrams of urea synthesis on TaCu@GDY, (b) Optimized intermediate configurations for urea synthesis on TaCu@GDY.

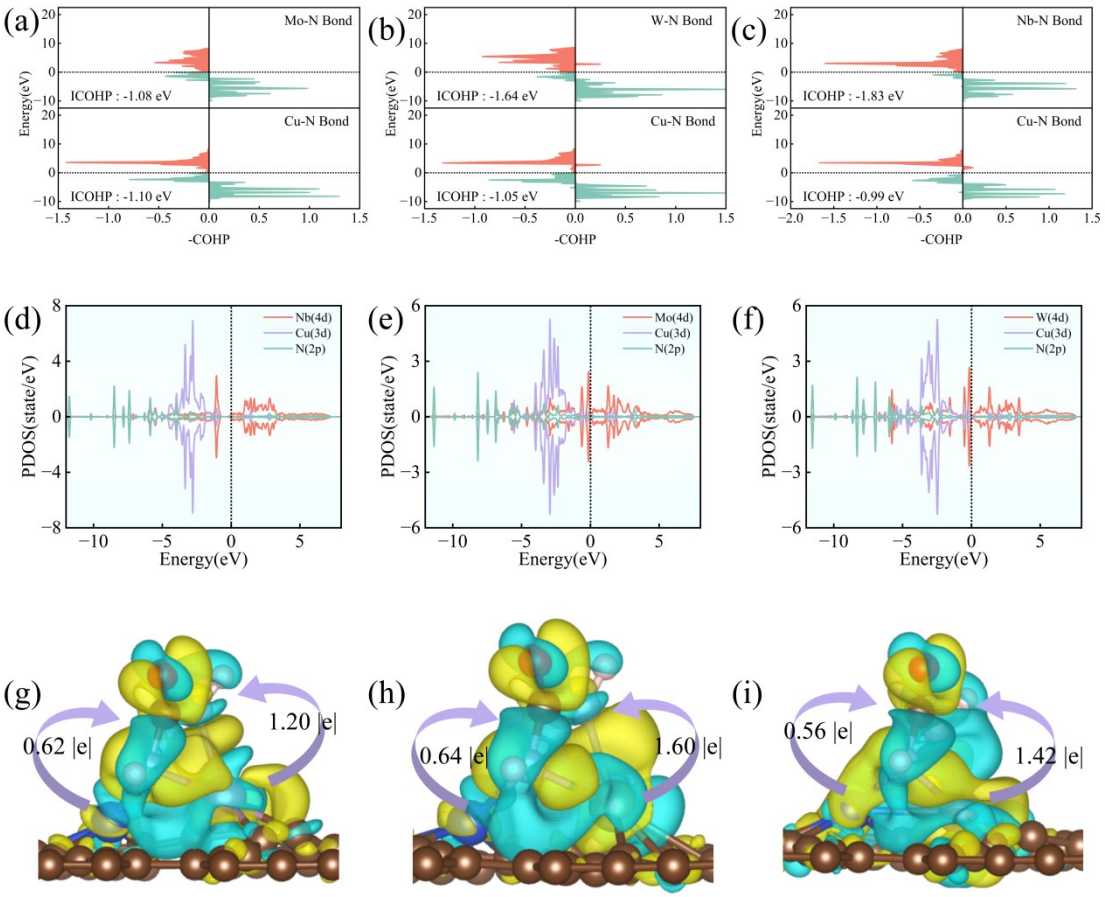

Figure S16. (a)-(c) Projected Crystal Orbital Hamiltonians (pCOHP) for TM-N and Cu-N interactions on MoCu@GDY, NbCu@GDY and WCu@GDY. (d) (f) (h) Projected density of states (PDOS) diagrams for *H_2NCONH adsorption on MoCu@GDY, NbCu@GDY, and WCu@GDY respectively. (e) (g) (i) Represent the charge density difference (CDD) of *H_2NCONH on MoCu@GDY, NbCu@GDY, and WCu@GDY respectively.

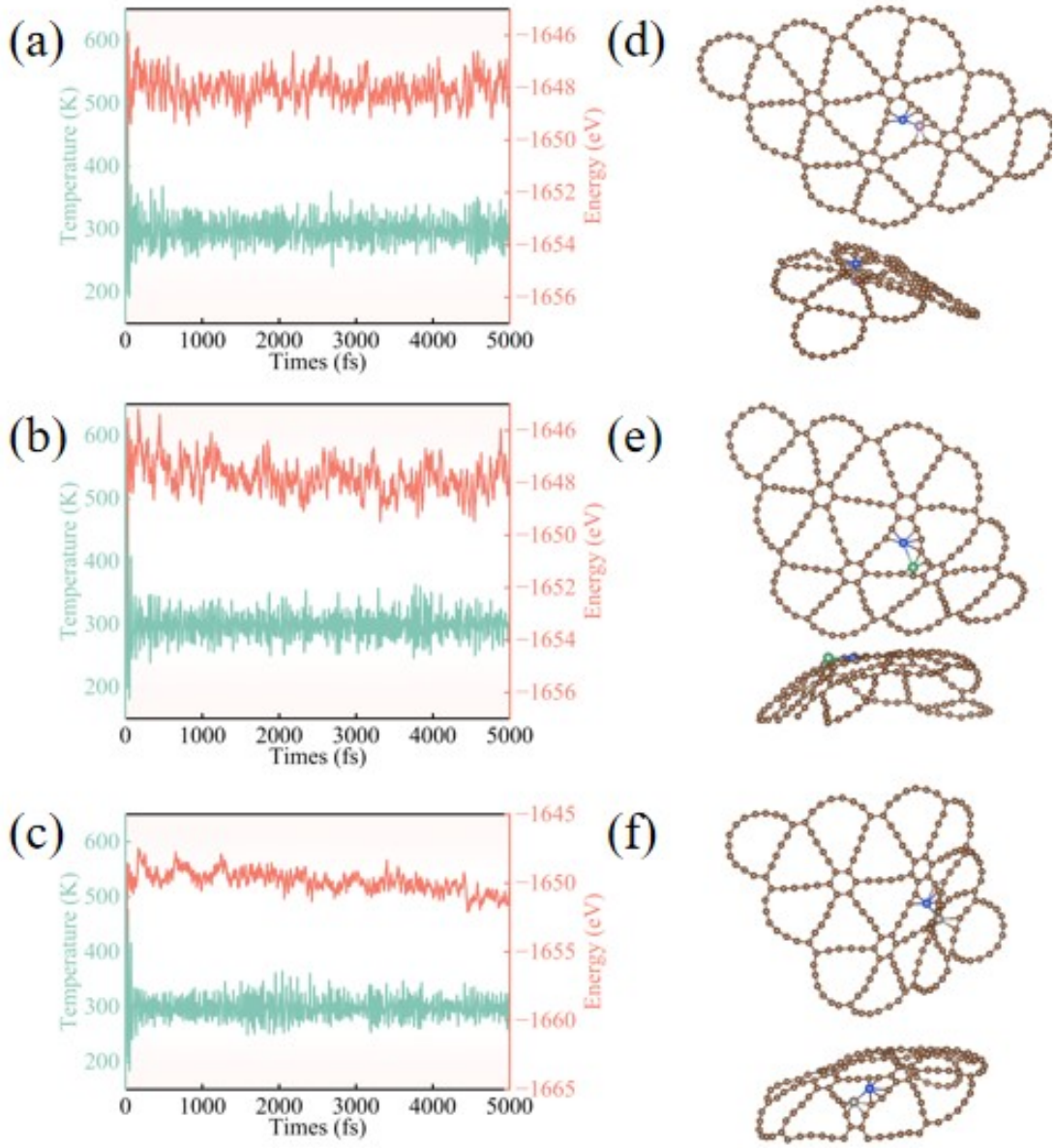

Figure S17. (a)-(c) present the AIMD simulation results for NbCu@GDY, MoCu@GDY, and WCu@GDY respectively, while (d)-(f) depict the final structures obtained from the AIMD simulations.

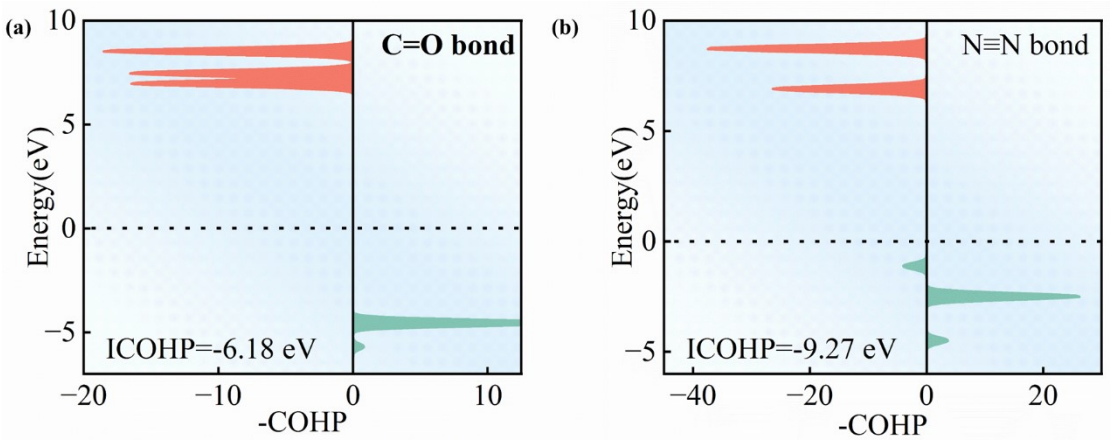

Figure S18. Projected Crystal Orbital Hamiltonian Population (pCOHP) for (a) C=O interactions of free CO_2 molecules and (b) N≡N interactions of free N_2 molecules.

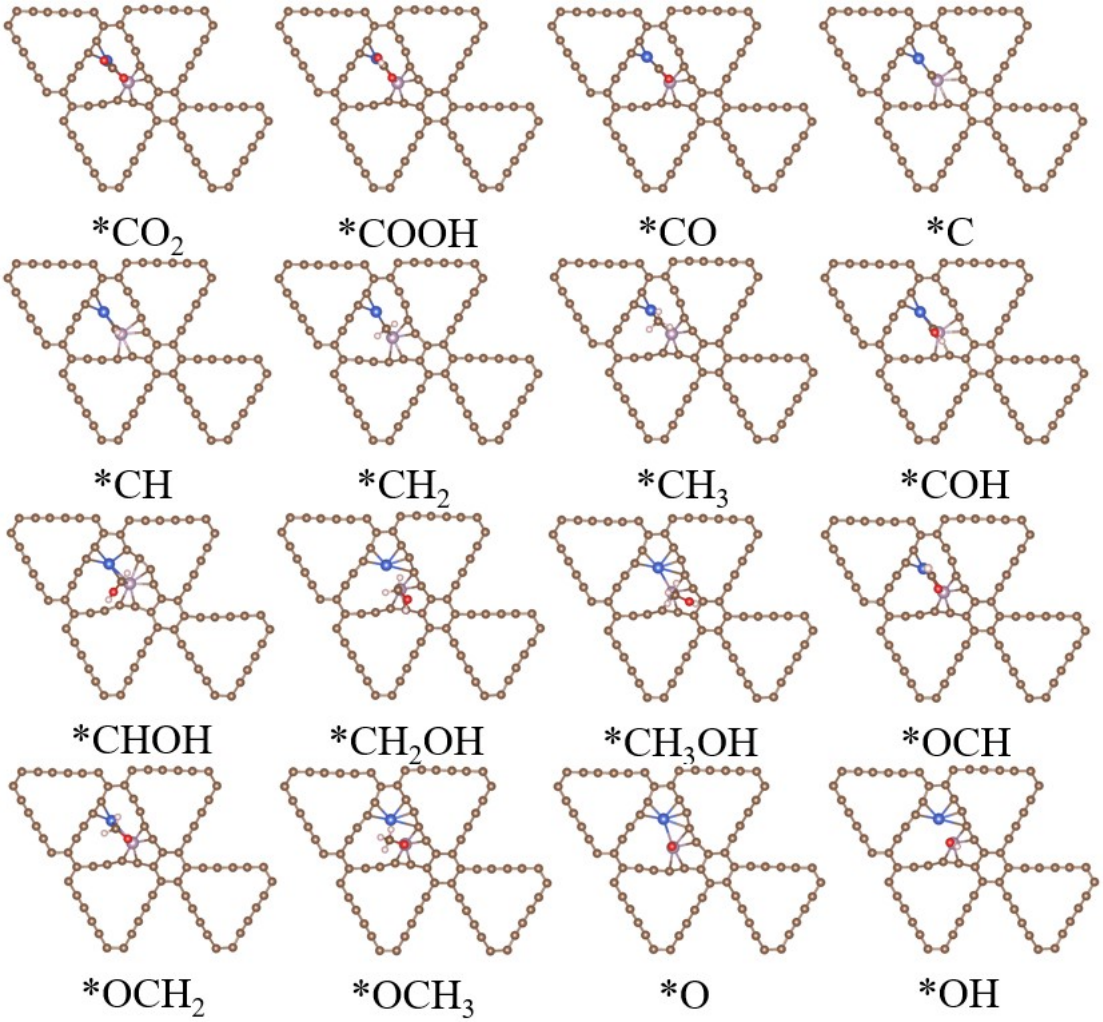

Figure S19. Optimized intermediate configurations for competitive CO_2RR reactions on MoCu@GDY.

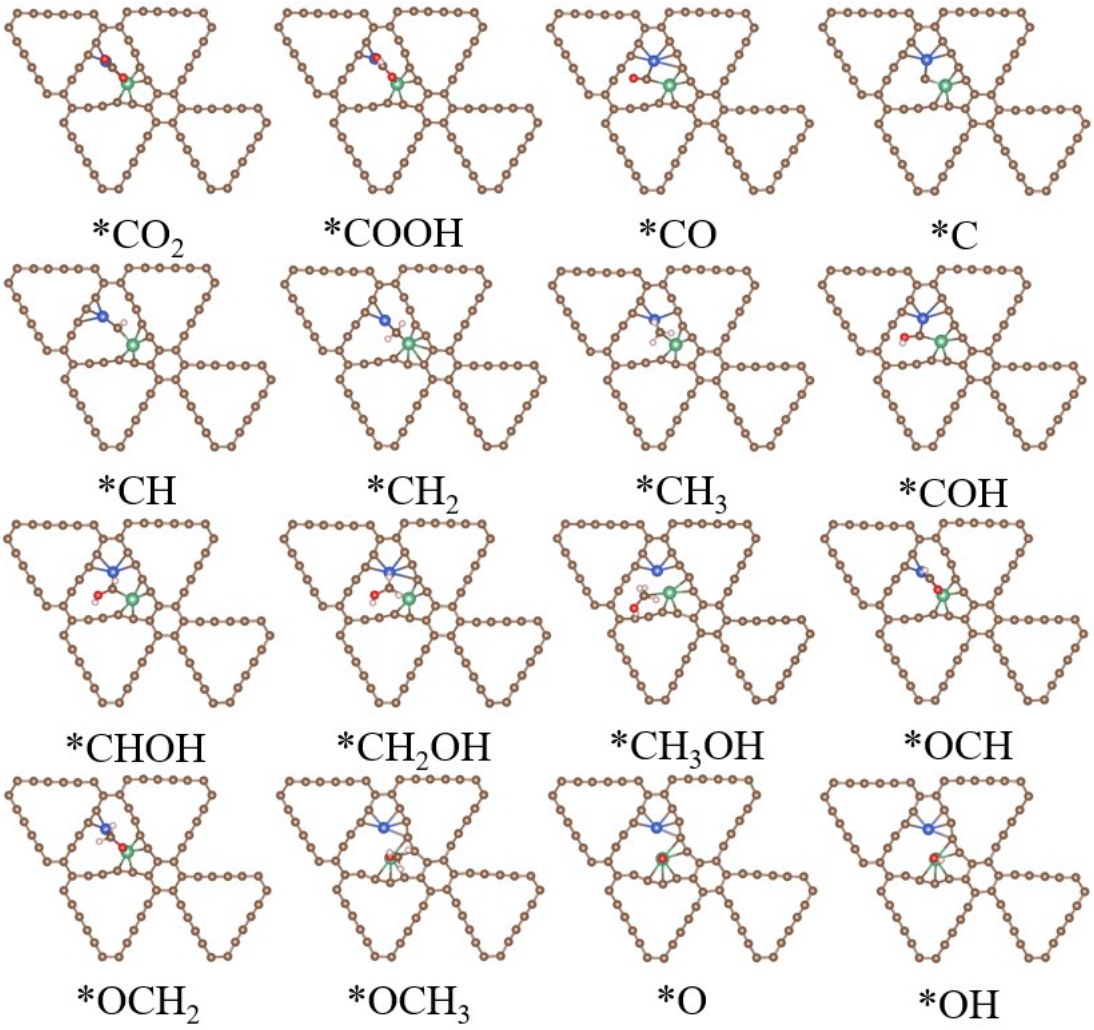

Figure S20. Optimized intermediate configurations for competitive CO_2RR reactions on NbCu@GDY.

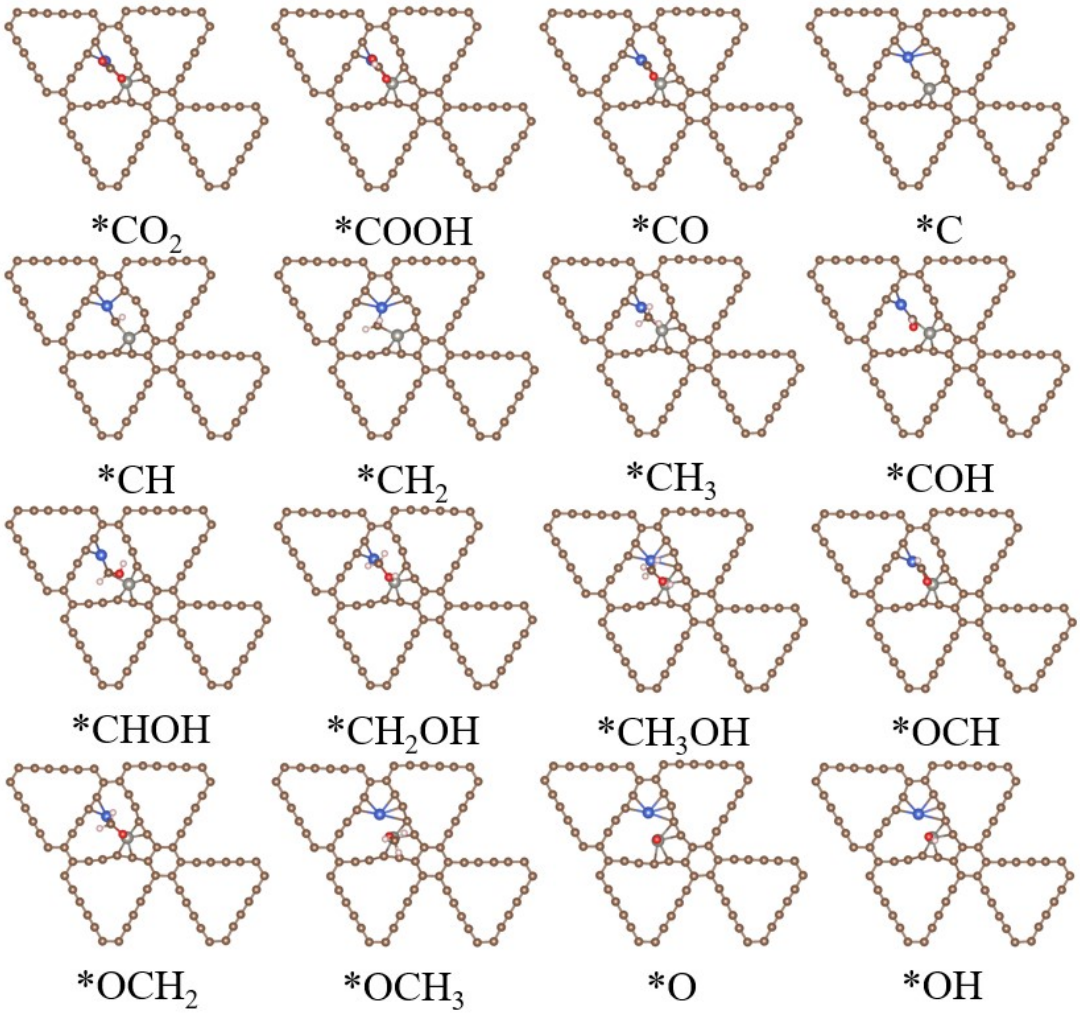

Figure S21. Optimized intermediate configurations for competitive CO_2RR reactions on WCu@GDY.

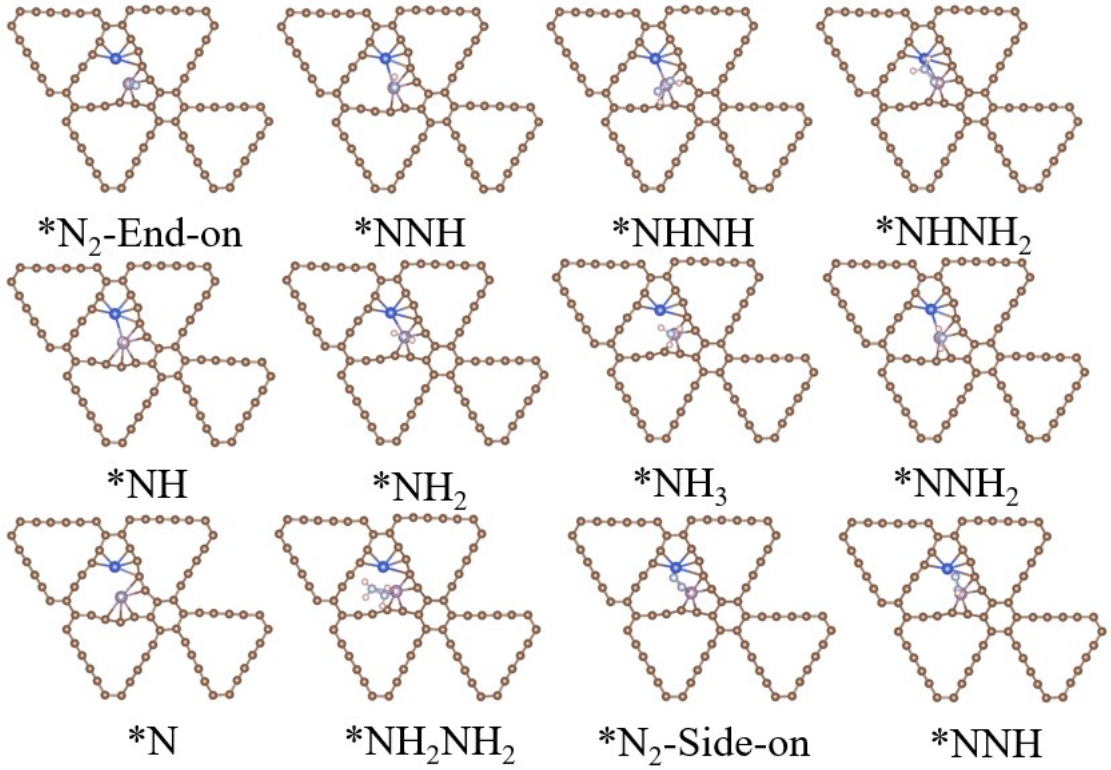

Figure S22. Optimized intermediate configurations for competitive reactions of NRR on MoCu@GDY.

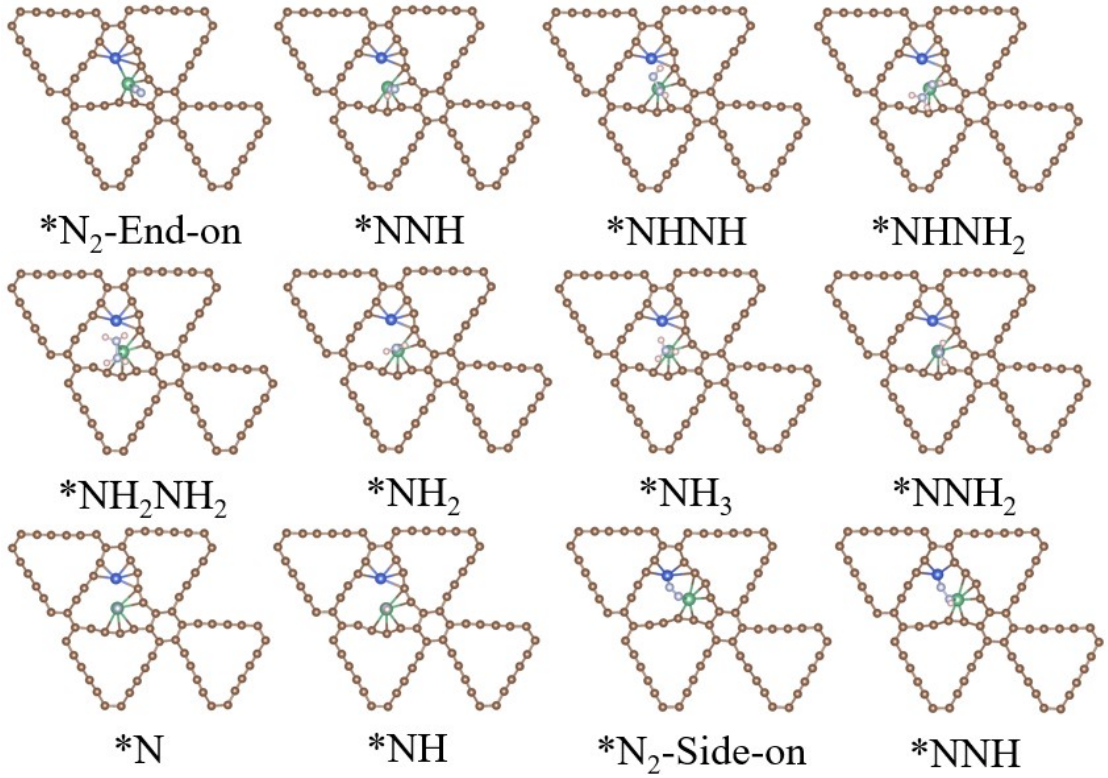

Figure S23. Optimized intermediate configurations for competitive reactions of NRR on NbCu@GDY.

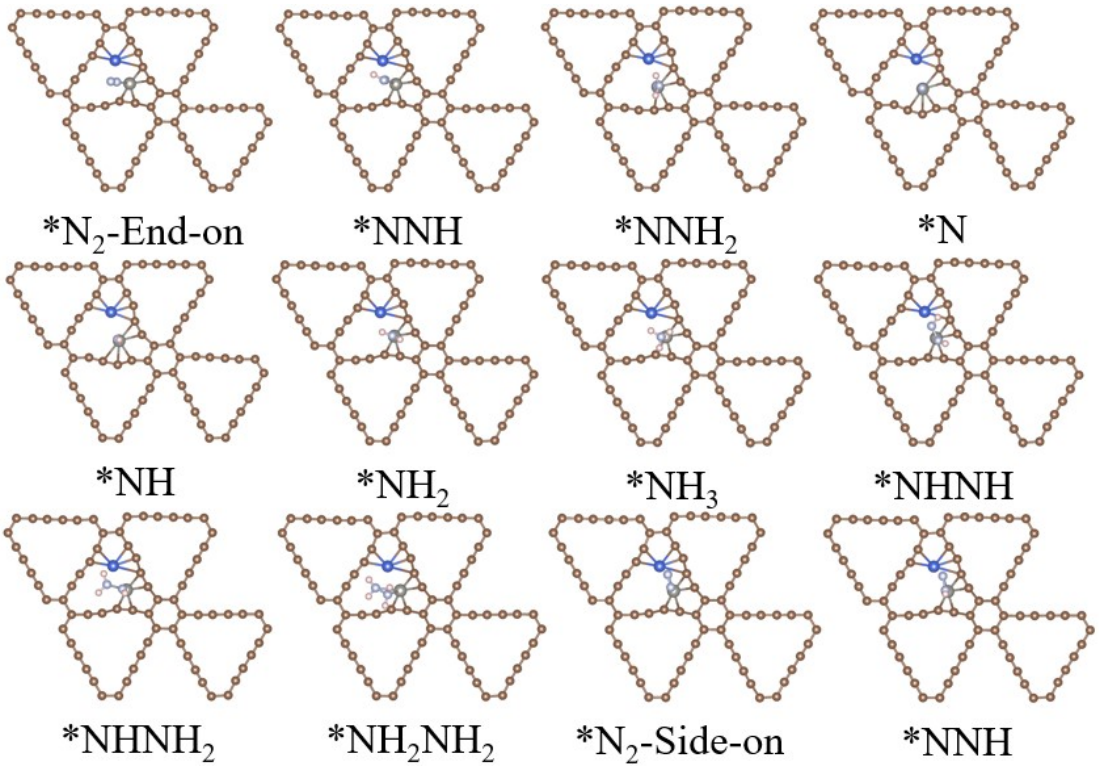

Figure S24. Optimized intermediate configurations for competitive reactions of NRR on WCu@GDY.

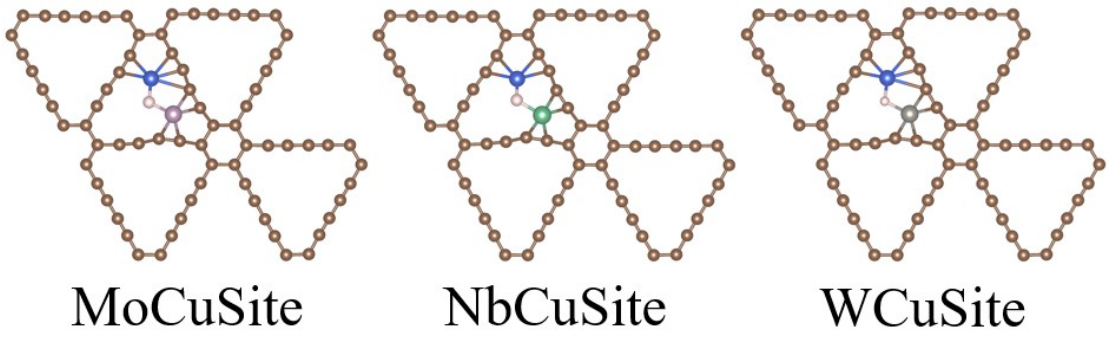

Figure S25. Optimized intermediate configurations for HER competition reactions on MoCu@GDY, NbCu@GDY and WCu@GDY.

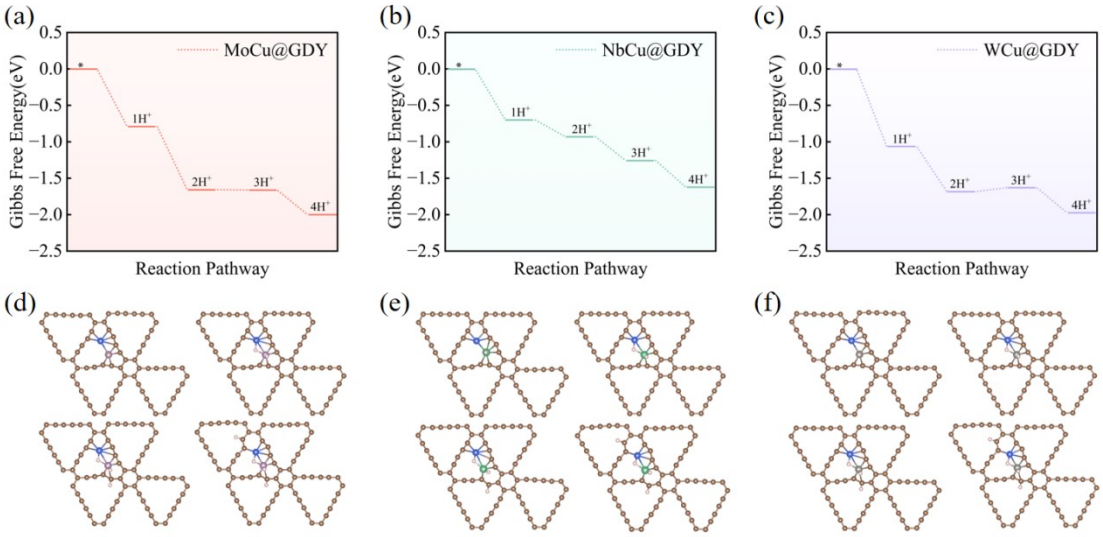

Figure S26. (a)-(c) Gibbs free energy step diagram for H at different concentrations covering TMCu@GDY. (d)-(f) Optimized intermediates in multi-step hydrogenation.

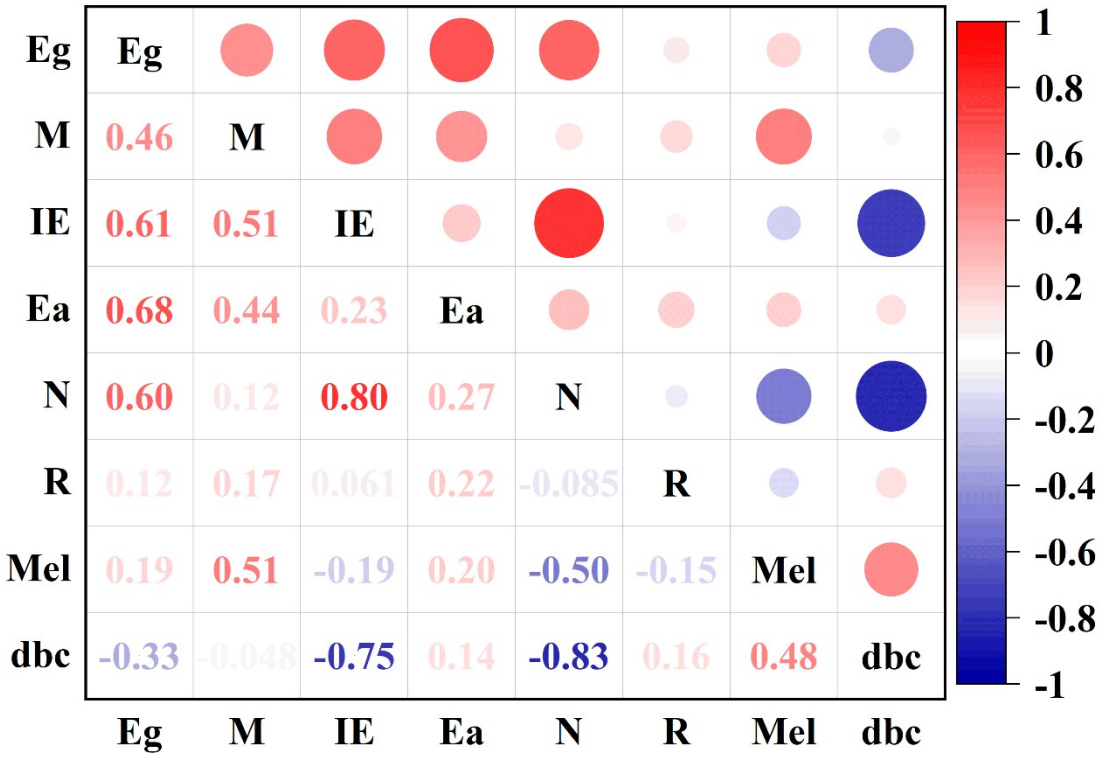

Figure S27. Heat map of Pearson correlation coefficient. Blue represents a positive correlation and red represents a negative correlation. The closer the absolute value is to 1, the stronger the correlation.

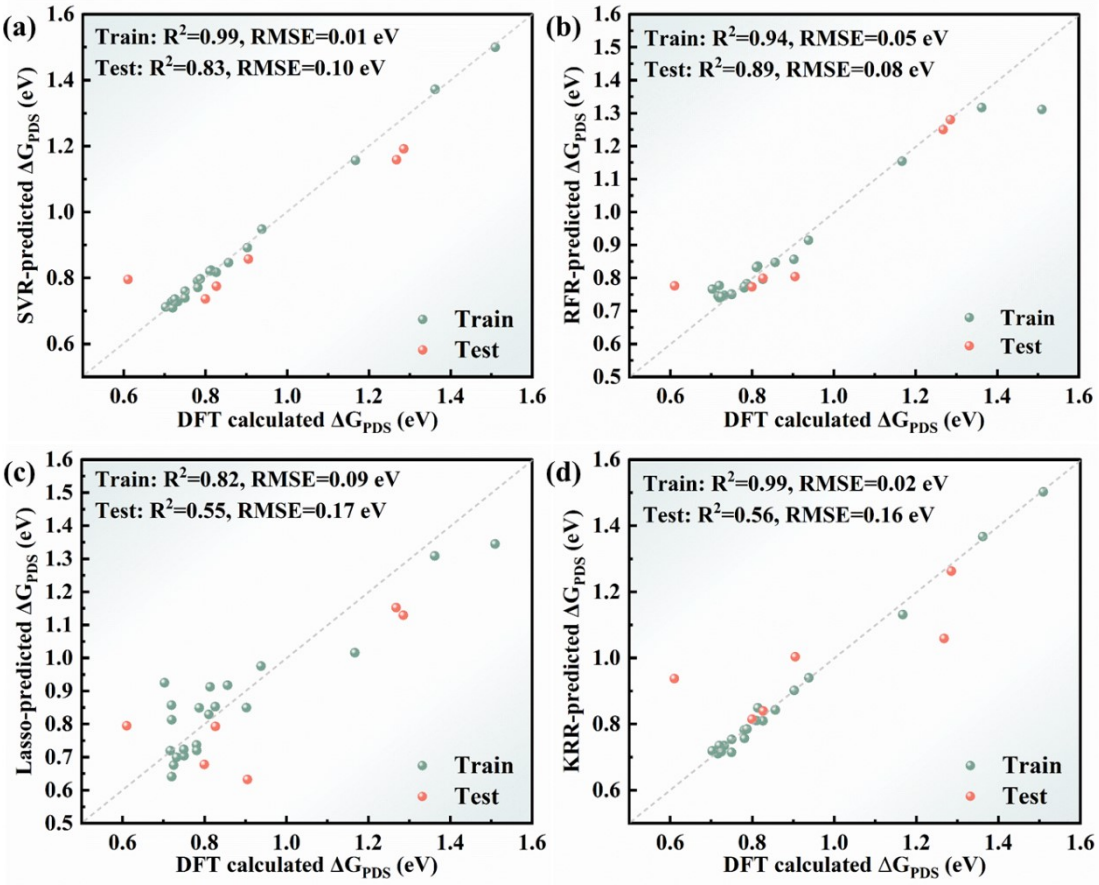

Figure S28. (a)-(d) Comparison of DFT with SVR, RFR, Lasso and KRR models for the predicted values of ΔG_{PDS}, respectively.

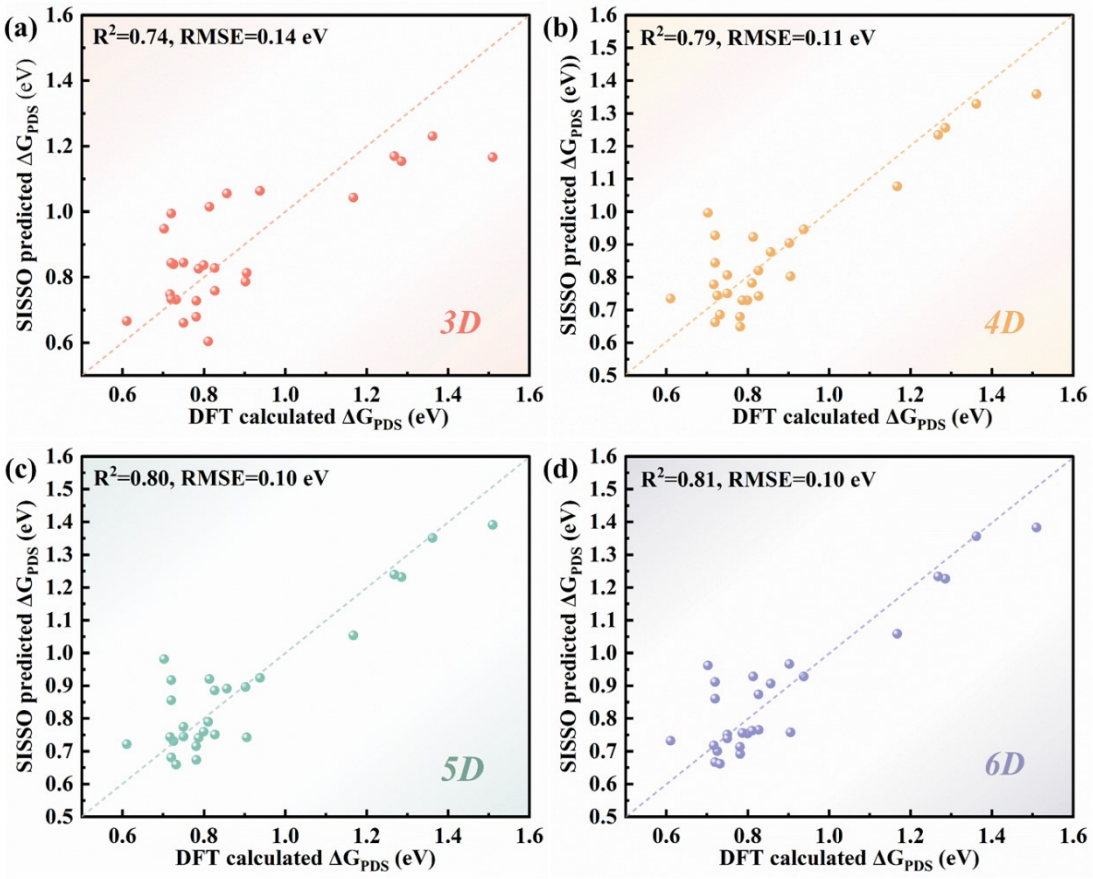

Figure S29. (a)-(d) Comparison of DFT and SISSO (3-6D) Prediction of values of ΔG_{PDS}, respectively.